

# Data report: permeabilities of Expedition 322 and 333 sediments from offshore the Kii Peninsula, Japan<sup>1</sup>

Elizabeth Screaton,<sup>2</sup> Katherine Rowe,<sup>2</sup> James Sutton,<sup>2</sup> and Gokce Atalan<sup>2</sup>

## Chapter contents

<a href="#">Abstract</a> .....	1
<a href="#">Introduction</a> .....	1
<a href="#">Methods</a> .....	1
<a href="#">Results</a> .....	3
<a href="#">Acknowledgments</a> .....	3
<a href="#">References</a> .....	3
<a href="#">Figures</a> .....	5
<a href="#">Table</a> .....	8

## Abstract

Permeability tests were conducted on core samples from Integrated Ocean Drilling Program Expeditions 322 and 333, which investigated the Kumano transect offshore the Kii Peninsula, Japan. Samples from Sites C0011 and C0012 represent Shikoku Basin sediments from the incoming plate, whereas the sample from Site C0018 represents slope sediments in the megasplay fault region. Measured vertical permeabilities vary from  $1.3 \times 10^{-19}$  to  $2.8 \times 10^{-16}$  m<sup>2</sup>.

## Introduction

Integrated Ocean Drilling Program (IODP) Expeditions 322 and 333 are part of a multistage, multiexpedition effort known as the Nankai Trough Seismogenic Zone Experiment (NanTroSEIZE). NanTroSEIZE focuses on drilling, sampling, and placing instruments to understand seismogenic mechanisms and faulting within the Nankai Trough subduction zone.

In this study, we used flow-through permeability tests to measure the vertical permeability of core samples from IODP Sites C0011, C0012, and C0018. Permeability of the incoming sediments (Sites C0011 and C0012; Fig. F1) impacts the response of the sediments to increasing total stress as they are subducted or accreted, as well as the transmittal of fluids from beneath the accretionary prism and the alteration of the subducting basaltic crust. Recovered sediments from Sites C0011 and C0012 are composed of pelagic and hemipelagic mud, with some volcanic ash and silty, sandy, and volcanoclastic turbidites (see the “[Site C0011](#)” and “[Site C0012](#)” chapters [Expedition 322 Scientists, 2010a, 2010b]; Expedition 333 Scientists, 2012b, 2012c, 2012d). Permeability of sediments in the megasplay fault region impacts pore pressure generation and may affect slope stability. The sample from Site C0018 consists of slope sediment from the megasplay region from within an interval identified as a mass transport deposit (Expedition 333 Scientists, 2012d).

## Methods

Permeability tests were conducted using the Trautwein Soil Testing Equipment Company’s DigiFlow K (Fig. F2). The equipment consists of a cell (to contain the sample and provide isostatic

<sup>1</sup>Screaton, E., Rowe, K., Sutton, J., and Atalan, G., 2013. Data report: permeabilities of Expedition 322 and 333 sediments from offshore the Kii Peninsula, Japan. *In* Saito, S., Underwood, M.B., Kubo, Y., and the Expedition 322 Scientists, *Proc. IODP, 322*: Tokyo (Integrated Ocean Drilling Program Management International, Inc.). doi:10.2204/iodp.proc.322.210.2013

<sup>2</sup>Department of Geological Sciences, University of Florida, Gainesville FL 32661, USA.  
Correspondence author: [screaton@ufl.edu](mailto:screaton@ufl.edu)



effective stress) and three pumps (sample top pump, sample bottom pump, and cell pump). Deionized water was used as the fluid in the pumps while an idealized solution of seawater (25 g NaCl and 8 g MgSO<sub>4</sub> per liter of water) permeated the sample. Pressure is transmitted from the deionized water in the top and bottom pumps to the permeant across rubber membranes in two interface chambers (Fig. F2).

The retrieved core samples from Expeditions 322 and 333 were stored in plastic core liners and sealed in aluminum bags during the expedition after sampling to prevent moisture loss. The sealed samples were stored in the refrigerator at 4°C until immediately prior to sample preparation. All testing was conducted with flow in the vertical direction (along the axis of the core). The permeability-testing apparatus accommodates the whole-round core. As a result, disturbance of the sample is minimal relative to testing during which plugs or subsamples are removed from the core. During preparation, the samples were carefully inspected for fracturing, disturbance, or signs of moisture loss (e.g., color change or cracking on outer surfaces). Two samples from Expedition 333 were not tested because of core damage. To provide freshly exposed surfaces, cores were trimmed on both ends using a wire saw or utility knife, depending on core properties. After trimming the ends of the sample, the diameter and height of the sample were measured. Sample diameters ranged from 5.7 to 6.5 cm, and sample heights varied from ~5.4 to 9.9 cm. The sample was then placed in a rubber membrane and fitted with saturated porous disks on both ends. The porous disks have been tested in the permeameter to ensure that they do not reduce flow and impact permeability calculations. Tests indicate that permeability of the disks is significantly >10<sup>-14</sup> m<sup>2</sup>.

The sample was placed in the cell, which was filled with deionized water so that the membrane-encased sample was completely surrounded by fluid. A small confining pressure of ~0.03 MPa (5 psi) was applied, and flow lines were flushed to remove any trapped air bubbles. After flushing the flow lines, the sample was backpressured to ~0.28 MPa (40 psi). Backpressure was achieved by concurrently ramping the cell pressure and the sample pressure to maintain a steady effective stress of 0.03 MPa. Because the whole-round samples were sealed immediately after cutting the core liner, the samples were expected to be near saturation prior to testing. Backpressuring at 0.28 MPa (40 psi) for ~24 h is sufficient to ensure full saturation under these conditions (ASTM, 1990). After backpressure, the cell fluid pressure was increased while the sample backpressure was maintained, thus increasing the effective stress on the sample. This effective stress both consolidates the sample and

pushes the flexible membrane against the sample to prevent flow bypassing the sample. Previous results from this laboratory have been consistent with results from fixed-wall consolidation cells (see fig. 6 in Skarbek and Saffer, 2009).

Once the target effective stress was achieved, the sample was allowed to equilibrate for at least 12 h and generally 24 h. Throughout testing, inflows and outflows to the cell fluid were monitored to assess changes in sample volume. Sample data were recorded every 1 min. Because fluid pressure in the closed hydraulic system can be affected by temperature changes, testing was conducted within a closed cabinet with a fan to keep the internal temperature uniform. The temperature was maintained at ~30°C (±1°C) during flow tests and consolidation steps. As many as three flow tests were performed at each effective stress level, with flow direction varied between tests. Flow tests were run by specifying pressures of the top and bottom pump and allowing flow rates into and out of the sample to equilibrate with time. Equilibrium was indicated by consistency between inflow and outflow rates. Pump pressure transducer calibration indicates errors <0.004%.

We used the measured flow rate, cross-sectional area of the sample, and the head difference between the top and bottom of the sample to calculate the hydraulic conductivity using Darcy's law:

$$Q = -K \times A(\Delta h/\Delta l),$$

where

- Q = measured flow rate (in cubic meters per second),
- K = hydraulic conductivity (in meters per second),
- A = cross-sectional area of the sample (in square meters),
- Δh = difference in head across the sample (in meters), and
- Δl = length of the sample (in meters).

Hydraulic conductivity values were then converted to permeability (*k*; in square meters) using the following equation:

$$k = (K\mu)/(\rho g),$$

where

- ρ = fluid density (1023 kg/m<sup>3</sup>),
- g = the gravitational constant (9.81 m/s<sup>2</sup>), and
- μ = viscosity (0.000857 Pa.s).

The density value was estimated for a temperature of 30°C and a salinity of 33 kg/m<sup>3</sup> (Haynes, 2012). Assuming a reasonable water compressibility, density change because of the applied pressure is minor (<0.1%). The viscosity value was obtained from a

synthesis of previous relationships (Sharqawy et al., 2010) for water at a temperature of 30°C and salinity of 33 kg/m<sup>3</sup>. A 1 h interval of stable flow rates was averaged for the permeability calculations, and the standard deviation of the permeability during that interval was calculated to assess uncertainty. Fluctuations in the calculated permeability are likely caused by slight temperature variations. The resulting volume changes would cause temporary changes in measured flow rates. The time interval was selected based on where inflow best matched outflow, indicating steady-state conditions, and where the standard deviation of permeability was minimized.

For every sample, as many as three effective stress steps were performed, with effective stress conditions ranging from 0.14 to 0.55 MPa. The corresponding porosity for each effective stress was calculated using the change in volume of fluid (mL) contained in the cell during each consolidation step. Total sample volume ( $V_{T(0)}$ ) was calculated using the following equation:

$$V_{T(0)} = \pi r^2 h,$$

where

$r$  = radius of the core sample, and

$h$  = height of the sample.

Initial porosities ( $n_0$ ) for volume calculations were obtained from shipboard moisture and density results of samples that were taken immediately adjacent to each whole-round sample collected for permeability testing. We assumed that the porosity of the sample at the end of backpressure is similar to the  $n_0$  of the sample because of the small change in effective stress (0.03 MPa).

Using  $n_0$ , the volume of voids before testing ( $V_{V(0)}$ ) was calculated:

$$V_{V(0)} = n_0 V_{T(0)}.$$

Volume of solids ( $V_s$ ) was calculated using the following equation:

$$V_s = V_{T(0)} - V_{V(0)}.$$

Using the difference of cell volumes between two consecutive steps (e.g., cell volume at backpressure and cell volume at first consolidation), the change in volume of water in the cell ( $\Delta V_{T(1)}$ ) was calculated. The new total volume of the sample ( $V_{T(1)}$ ) after pore spaces were reduced during the consolidation process was determined by subtracting the change in cell volume at the end of the consolidation step ( $\Delta V_{T(1)}$ ) from the total sample volume ( $V_{T(0)}$ ):

$$V_{T(1)} = V_{T(0)} - \Delta V_{T(1)}.$$

Using the calculated new total volume of the sample ( $V_{T(1)}$ ), the new porosity at the end of the consolidation is calculated. The new porosity ( $n_1$ ) at the end of the consolidation is

$$n_1 = (1 - V_s)/V_{T(1)}.$$

## Results

Table T1 summarizes the effective stress and estimated porosity and permeability at each consolidation step. Permeability is plotted as a function of porosity on Figure F3, with samples noted that were observed to contain primarily sand or ash. Permeabilities where the standard deviation exceeded 10% of the value are italicized in Table T1 and are not plotted on Figure F3. For comparison, Figure F3 also shows the permeability-porosity relationship developed by Skarbek and Saffer (2009) for hemipelagic mud of the Shikoku Basin facies sediments from Ocean Drilling Program (ODP) Sites 1173 and 1174 on the Muroto transect ( $\log(k) = -20.45 + 6.93n$ ). With the exception of three samples, two of which were noted to contain sand-sized material and one which was slope sediments of Site C0018, permeabilities generally fall near or below that indicated by the Skarbek and Saffer (2009) relationship. Measured vertical permeabilities vary from  $\sim 1.3 \times 10^{-19}$  to  $\sim 2.8 \times 10^{-16}$  m<sup>2</sup>.

## Acknowledgments

This research used samples and data provided by the Integrated Ocean Drilling Program (IODP). Funding for Expedition 333 postcruise research was provided by a Consortium of Ocean Leadership U.S. Science Support Program grant to Screaton.

## References

- ASTM International, 1990. Standard test method for measurement of hydraulic conductivity of saturated porous materials using a flexible wall permeameter (Standard D5084–70). In *Annual Book of ASTM Standards*: Philadelphia (Am. Soc. Testing Mater.), 63–70.
- Expedition 322 Scientists, 2010a. Site C0011. In Saito, S., Underwood, M.B., Kubo, Y., and the Expedition 322 Scientists, *Proc. IODP, 322*: Tokyo (Integrated Ocean Drilling Program Management International, Inc.). [doi:10.2204/iodp.proc.322.103.2010](https://doi.org/10.2204/iodp.proc.322.103.2010)
- Expedition 322 Scientists, 2010b. Site C0012. In Saito, S., Underwood, M.B., Kubo, Y., and the Expedition 322 Scientists, *Proc. IODP, 322*: Tokyo (Integrated Ocean Drilling Program Management International, Inc.). [doi:10.2204/iodp.proc.322.104.2010](https://doi.org/10.2204/iodp.proc.322.104.2010)

- Expedition 333 Scientists, 2012a. Methods. *In* Henry, P., Kanamatsu, T., Moe, K., and the Expedition 333 Scientists, *Proc. IODP*, 333: Tokyo (Integrated Ocean Drilling Program Management International, Inc.). [doi:10.2204/iodp.proc.333.102.2012](https://doi.org/10.2204/iodp.proc.333.102.2012)
- Expedition 333 Scientists, 2012b. Site C0011. *In* Henry, P., Kanamatsu, T., Moe, K., and the Expedition 333 Scientists, *Proc. IODP*, 333: Tokyo (Integrated Ocean Drilling Program Management International, Inc.). [doi:10.2204/iodp.proc.333.104.2012](https://doi.org/10.2204/iodp.proc.333.104.2012)
- Expedition 333 Scientists, 2012c. Site C0012. *In* Henry, P., Kanamatsu, T., Moe, K., and the Expedition 333 Scientists, *Proc. IODP*, 333: Tokyo (Integrated Ocean Drilling Program Management International, Inc.). [doi:10.2204/iodp.proc.333.105.2012](https://doi.org/10.2204/iodp.proc.333.105.2012)
- Expedition 333 Scientists, 2012d. Site C0018. *In* Henry, P., Kanamatsu, T., Moe, K., and the Expedition 333 Scientists, *Proc. IODP*, 333: Tokyo (Integrated Ocean Drilling Program Management International, Inc.). [doi:10.2204/iodp.proc.333.103.2012](https://doi.org/10.2204/iodp.proc.333.103.2012)
- Haynes, W.M. (Ed.), 2012. *CRC Handbook of Chemistry and Physics* (93rd ed.): Boca Raton (CRC Press).
- Moore, G.F., Park, J.-O., Bangs, N.L., Gulick, S.P., Tobin, H.J., Nakamura, Y., Sato, S., Tsuji, T., Yoro, T., Tanaka, H., Uraki, S., Kido, Y., Sanada, Y., Kuramoto, S., and Taira, A., 2009. Structural and seismic stratigraphic framework of the NanTroSEIZE Stage 1 transect. *In* Kinoshita, M., Tobin, H., Ashi, J., Kimura, G., Lallemand, S., Screaton, E.J., Curewitz, D., Masago, H., Moe, K.T., and the Expedition 314/315/316 Scientists, *Proc. IODP*, 314/315/316: Washington, DC (Integrated Ocean Drilling Program Management International, Inc.). [doi:10.2204/iodp.proc.314315316.102.2009](https://doi.org/10.2204/iodp.proc.314315316.102.2009)
- Sharqawy, M.H., Lienhard, J.H., V, and Zubair, S.M., 2010. Thermophysical properties of seawater: a review of existing correlations and data. *Desalin. Water Treat.*, 16(1–3):354–380. [doi:10.5004/dwt.2010.1079](https://doi.org/10.5004/dwt.2010.1079)
- Skarbek, R.M., and Saffer, D.M., 2009. Pore pressure development beneath the décollement at the Nankai subduction zone: implications for plate boundary fault strength and sediment dewatering. *J. Geophys. Res.: Solid Earth*, 114(B7):B07401. [doi:10.1029/2008JB006205](https://doi.org/10.1029/2008JB006205)
- Initial receipt:** 27 February 2013  
**Acceptance:** 14 June 2013  
**Publication:** 23 August 2013  
**MS 322-210**

**Figure F1.** Location of Nankai Trough and Kumano transect sites, Expeditions 322 and 333 (modified from Moore et al., 2009). Previously drilled ODP Sites 1173 and 1174 on the Muroto transect also shown.

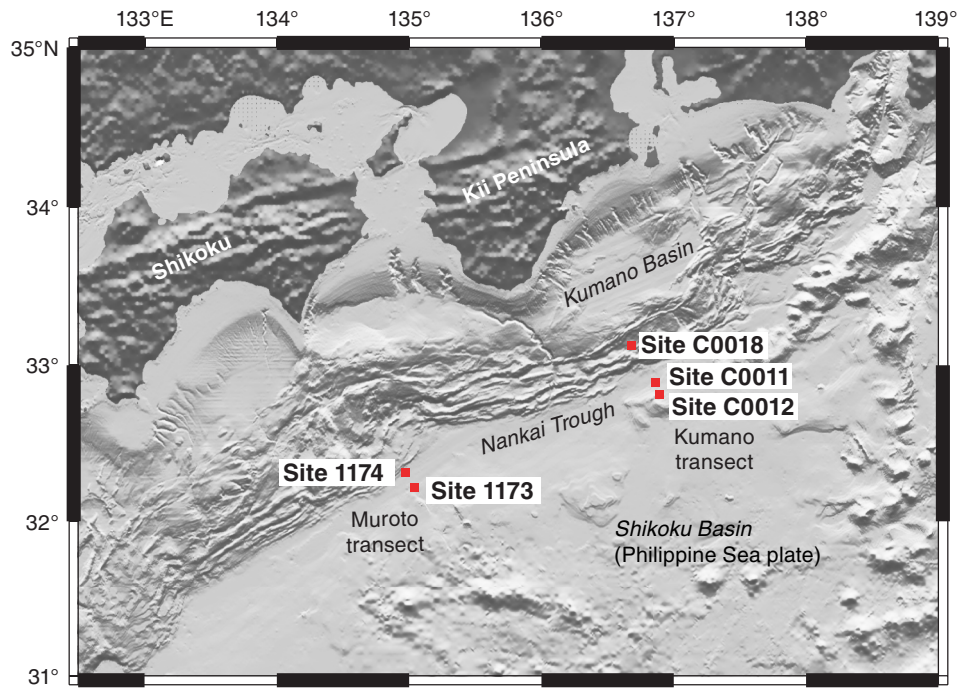


**Figure F2.** A. Schematic of the permeability test system. B. Labeled photo of the permeability test system. The top, bottom, and cell pumps from Geotac consist of 80 mL pistons that are moved upward or downward to infuse or extract water from the sample or cell. The 160 mL interface chamber has a rubber diaphragm in the center, which separates the saltwater that is used as a permeant (bottom chamber) from the distilled water used in the pumps (top chamber). Deionized (DI) water is used in the cell pump and in the sample cell, which has a volume of 2300 mL.

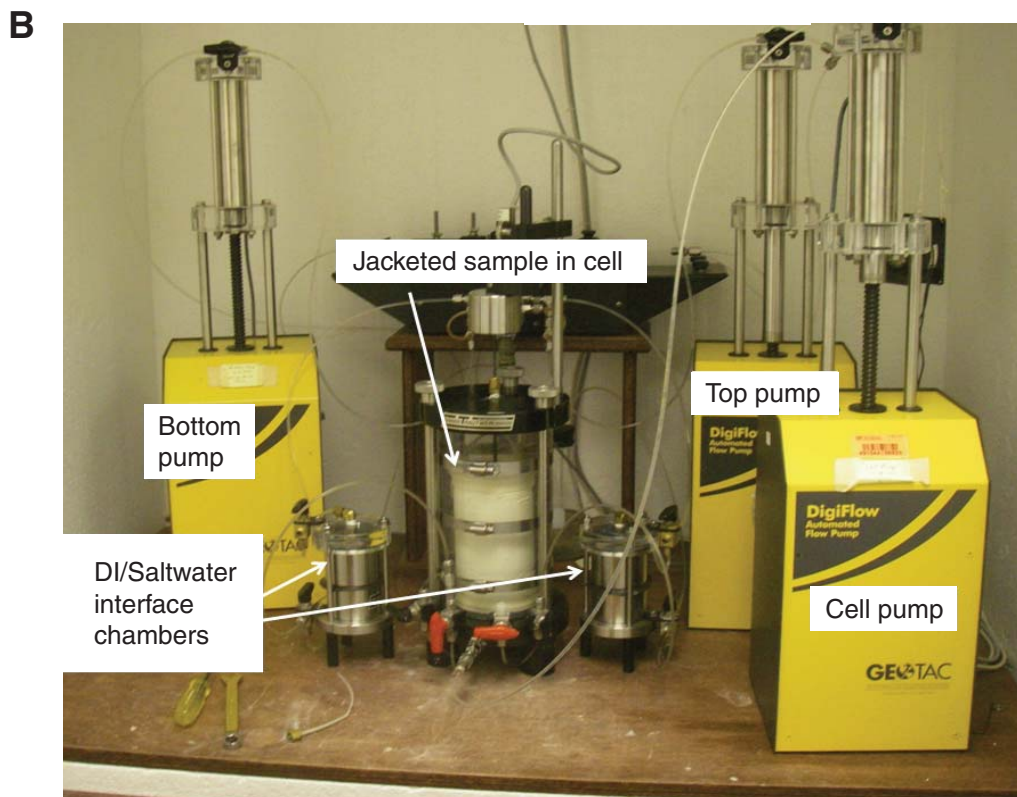
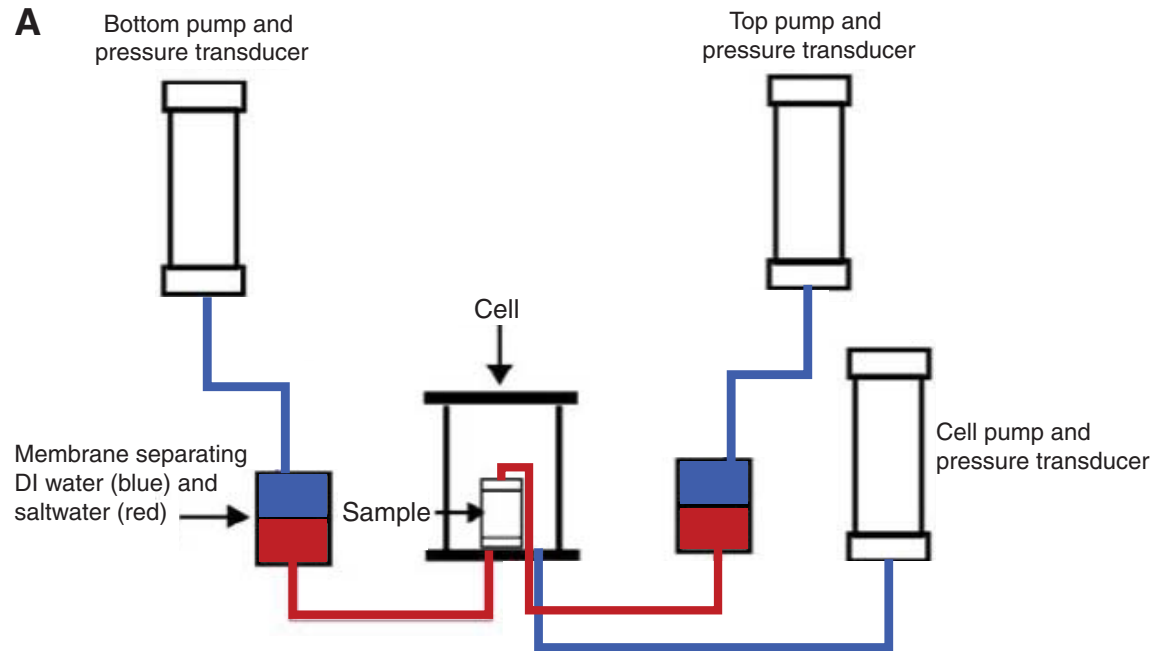


**Figure F3.** Measured permeability as a function of porosity. Open symbols = samples that were observed to contain significant sand-sized material, solid symbols = clay or silt-dominated samples.

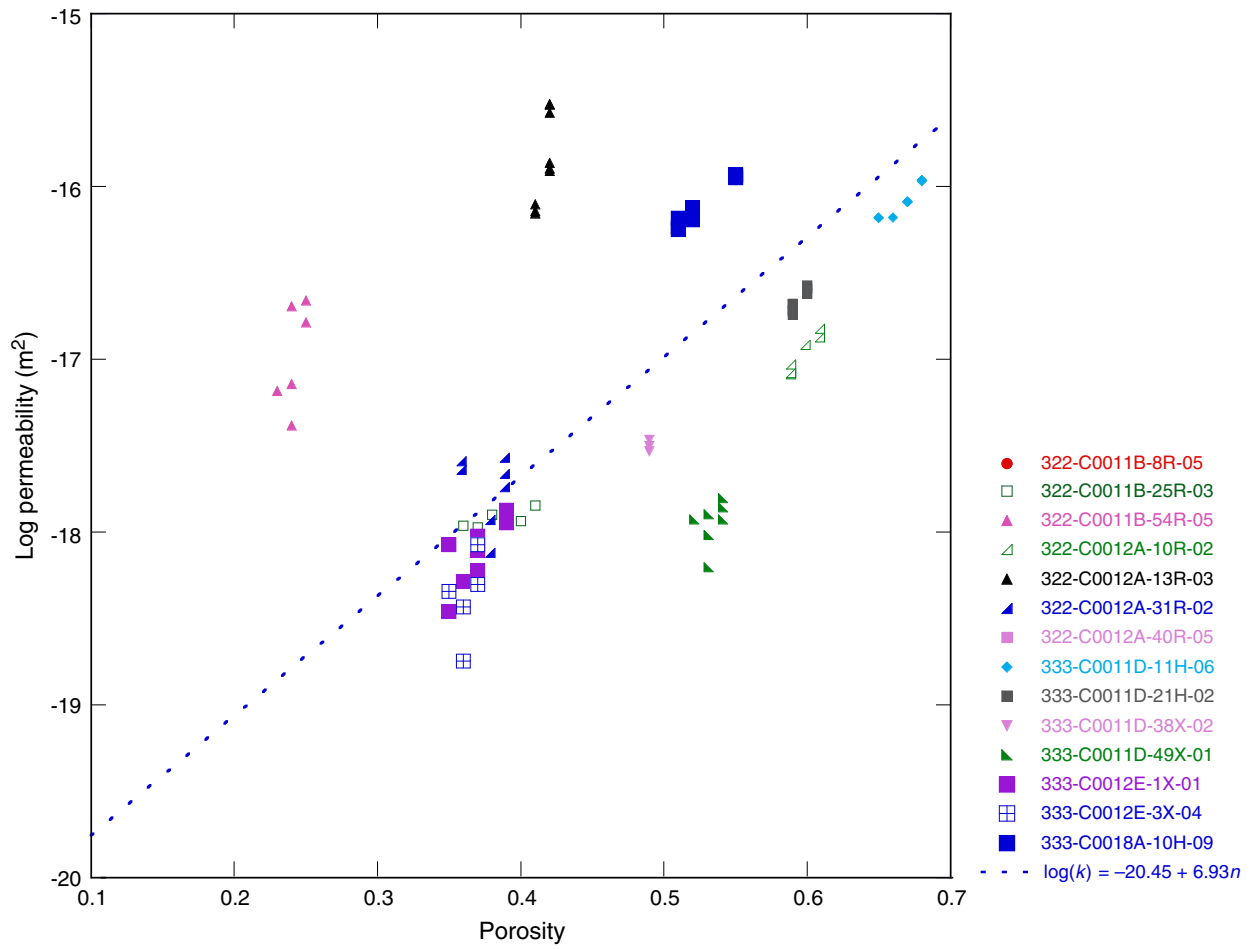




**Table T1.** Results from laboratory permeability tests, Expeditions 322 and 333. (Continued on next two pages.)

Core, section	Unit/Subunit	Facies	Lithology	Top depth (mbsf)	Diameter (m)	Length (m)	Initial porosity	Confining pressure (MPa)	Top pressure (MPa)	Bottom pressure (MPa)	Effective stress (MPa)	Test	Computed porosity	Flow rate (mL/min)	$\Delta h$ (m)	Hydraulic conductivity (m/s)	Permeability (m <sup>2</sup> )	Standard deviation of k (m <sup>2</sup> )								
322-C0011B-8R-5	II	Volcanic turbidite	Silty clay	408.47	0.06	0.09	0.52	0.41	0.27	0.28	0.14	1	0.51	1.37E-04	-1.5	5.64E-11	4.82E-18	9.31E-20								
								0.41	0.29	0.27	0.14	2	0.51	-1.86E-04	2.0	5.70E-11	4.87E-18	5.36E-20								
								0.41	0.26	0.29	0.14	3	0.51	2.96E-04	-2.8	6.29E-11	5.37E-18	3.51E-20								
								0.55	0.28	0.27	0.28	1	0.50	-1.00E-04	1.3	4.70E-11	4.02E-18	4.10E-19								
								0.55	0.27	0.29	0.28	2	0.50	1.45E-04	-2.2	4.06E-11	3.46E-18	5.05E-20								
								0.55	0.29	0.26	0.28	3	0.50	-1.84E-04	2.7	4.17E-11	3.56E-18	5.42E-20								
								0.69	0.27	0.28	0.41	1	0.49	8.09E-05	-1.5	3.34E-11	2.85E-18	6.64E-20								
								0.69	0.29	0.27	0.41	2	0.49	-1.27E-04	2.0	3.88E-11	3.32E-18	1.28E-19								
								0.69	0.26	0.29	0.41	3	0.49	1.54E-04	-2.8	3.28E-11	2.80E-18	5.46E-20								
								25R-3	III	Hemipelagic	Silty clay	540.49	0.06	0.07	0.42	0.41	0.29	0.26	0.14	1	0.41	-9.76E-05	2.7	1.67E-11	1.43E-18	1.05E-19
0.41	0.28	0.27	0.14	2	0.40	-4.32E-05	1.3									1.53E-11	1.31E-18	1.75E-19								
0.41	0.26	0.30	0.14	3	0.40	1.25E-04	-4.2									1.35E-11	1.16E-18	3.27E-20								
0.55	0.28	0.27	0.28	1	0.39	-4.27E-05	1.3									1.52E-11	1.29E-18	1.91E-19								
0.55	0.26	0.29	0.28	2	0.39	8.98E-05	-2.8									1.44E-11	1.23E-18	6.46E-19								
0.55	0.30	0.26	0.28	3	0.38	-1.30E-04	4.0									1.47E-11	1.26E-18	8.91E-20								
0.69	0.30	0.26	0.41	1	0.37	-1.10E-04	4.0									1.24E-11	1.06E-18	9.07E-20								
0.69	0.27	0.28	0.41	2	0.36	1.17E-05	-1.5									3.65E-12	3.11E-19	1.38E-19								
0.69	0.29	0.26	0.41	3	0.36	-7.43E-05	2.7									1.27E-11	1.09E-18	9.94E-20								
54R-5	IV	Silty turbidite	Clayey silt with sand	775.355	0.06	0.09	0.31									0.41	0.28	0.27	0.14	1	0.25	-4.10E-04	1.3	1.91E-10	1.63E-17	4.22E-19
								0.41	0.27	0.29	0.14	2	0.25	9.23E-04	-2.2	2.57E-10	2.20E-17	1.59E-19								
								0.41	0.26	0.29	0.14	3	0.24	1.13E-03	-2.8	2.38E-10	2.03E-17	3.98E-19								
								0.55	0.27	0.28	0.28	1	0.24	2.06E-04	-1.5	8.45E-11	7.22E-18	1.19E-19								
								0.55	0.29	0.27	0.28	2	0.24	-1.60E-04	2.0	4.86E-11	4.15E-18	1.40E-19								
								0.55	0.26	0.29	0.28	3	0.23	3.64E-04	-2.8	7.69E-11	6.56E-18	5.92E-20								
								322-C0012A-10R-2	I	Hemipelagic/Pyroclastic	Silty clay	131.87	0.06	0.09	0.62	0.41	0.29	0.26	0.14	1	0.61	-8.00E-04	2.7	1.77E-10	1.51E-17	1.07E-19
0.41	0.28	0.27	0.14	2	0.61	-3.43E-04	1.3									1.57E-10	1.34E-17	2.10E-19								
0.41	0.26	0.30	0.14	3	0.60	1.01E-03	-4.2									1.42E-10	1.21E-17	1.61E-19								
0.55	0.28	0.27	0.28	1	0.59	-2.40E-04	1.3									1.10E-10	9.38E-18	3.42E-19								
0.55	0.26	0.30	0.28	2	0.59	6.90E-04	-4.2									9.63E-11	8.22E-18	1.09E-19								
0.55	0.29	0.26	0.28	3	0.59	-4.40E-04	2.7									9.73E-11	8.31E-18	9.43E-20								
13R-3	II	Volcanic turbidite	Clayey silt with sand	160.62	0.06	0.08	0.44									0.41	0.26	0.29	0.14	1	0.42	2.08E-02	-2.8	3.51E-09	2.99E-16	4.92E-18
																0.41	0.28	0.27	0.14	2	0.42	-9.39E-03	1.3	3.49E-09	2.98E-16	4.38E-18
																0.41	0.26	0.30	0.14	3	0.42	2.75E-02	-4.2	3.12E-09	2.66E-16	2.79E-18
																0.55	0.28	0.27	0.28	1	0.42	-4.32E-03	1.3	1.61E-09	1.37E-16	1.99E-18
								0.55	0.26	0.30	0.28	2	0.42	1.31E-02	-4.2	1.48E-09	1.27E-16	1.32E-18								
								0.55	0.29	0.26	0.28	3	0.42	-8.05E-03	2.7	1.45E-09	1.23E-16	9.72E-19								
								0.69	0.30	0.26	0.41	1	0.41	-7.78E-03	4.0	9.22E-10	7.87E-17	7.28E-19								
								0.69	0.27	0.28	0.41	2	0.41	2.50E-03	-1.5	8.17E-10	6.97E-17	7.98E-19								
								0.69	0.29	0.26	0.41	3	0.41	-4.68E-03	2.7	8.41E-10	7.18E-17	6.52E-19								
								31R-2	III	Hemipelagic	Clay	330.34	0.06	0.07	0.48	0.41	0.28	0.27	0.14	1	0.39	-9.15E-05	1.3	3.15E-11	2.69E-18	1.16E-19
0.41	0.27	0.29	0.14	2	0.39	1.24E-04	-2.2									2.54E-11	2.17E-18	7.60E-20								
0.41	0.29	0.26	0.14	3	0.39	-1.28E-04	2.7									2.13E-11	1.82E-18	5.39E-20								



Table T1 (continued). (Continued on next page.)

Core, section	Unit/Subunit	Facies	Lithology	Top depth (mbsf)	Diameter (m)	Length (m)	Initial porosity	Confining pressure (MPa)	Top pressure (MPa)	Bottom pressure (MPa)	Effective stress (MPa)	Test	Computed porosity	Flow rate (mL/min)	$\Delta h$ (m)	Hydraulic conductivity (m/s)	Permeability (m <sup>2</sup> )	Standard deviation of $k$ (m <sup>2</sup> )								
40R-5	V	Siliciclastic/Volcaniclastic turbidite	Clay	418.57	0.06	0.08	0.44	0.55	0.27	0.28	0.27	1	0.38	3.69E-05	-1.5	1.12E-11	9.54E-19	1.02E-19								
								0.55	0.29	0.27	0.27	2	0.38	-6.13E-05	2.0	1.37E-11	1.17E-18	8.51E-20								
								0.55	0.26	0.29	0.27	3	0.38	5.73E-05	-2.8	8.93E-12	7.62E-19	3.63E-20								
								0.69	0.28	0.27	0.41	1	0.36	-8.79E-05	1.3	3.03E-11	2.58E-18	1.51E-19								
								0.69	0.29	0.26	0.41	2	0.36	-1.61E-04	2.7	2.68E-11	2.29E-18	4.46E-20								
								0.41	0.28	0.27	0.14	1	0.37	-1.31E-05	1.3	5.45E-12	4.65E-19	1.68E-19								
								0.41	0.27	0.29	0.14	2	0.37	3.37E-05	-2.2	8.40E-12	7.17E-19	9.04E-20								
								0.41	0.29	0.26	0.14	3	0.37	-3.26E-05	2.7	6.56E-12	5.60E-19	4.96E-20								
								333-C0011D-11H-6	I	Hemipelagic/Pyroclastic	Silty clay	105.465	0.06	0.09	0.69	0.41	0.28	0.27	0.14	1	0.68	-3.72E-03	1.3	1.28E-09	1.09E-16	6.46E-19
																0.41	0.27	0.29	0.14	2	0.68	6.15E-03	-2.2	1.26E-09	1.08E-16	7.84E-19
																0.41	0.29	0.26	0.14	3	0.68	-7.70E-03	2.7	1.27E-09	1.09E-16	7.07E-19
																0.55	0.27	0.28	0.28	1	0.67	3.17E-03	-1.5	9.55E-10	8.16E-17	5.04E-19
0.55	0.29	0.27	0.28	2	0.67	-4.31E-03	2.0									9.63E-10	8.23E-17	4.72E-19								
0.55	0.26	0.29	0.28	3	0.67	6.15E-03	-2.8									9.54E-10	8.15E-17	4.97E-19								
0.69	0.27	0.28	0.41	1	0.66	2.58E-03	-1.5									7.77E-10	6.63E-17	6.02E-19								
0.69	0.29	0.27	0.41	2	0.65	-3.47E-03	2.0									7.74E-10	6.61E-17	4.58E-19								
0.69	0.26	0.29	0.41	3	0.65	4.94E-03	-2.8									7.67E-10	6.55E-17	8.00E-19								
0.41	0.29	0.26	0.14	1	0.60	-1.74E-03	2.7									3.01E-10	2.57E-17	2.85E-19								
0.41	0.27	0.28	0.14	2	0.60	8.96E-04	-1.5									2.82E-10	2.41E-17	4.43E-19								
0.41	0.26	0.30	0.14	3	0.60	2.87E-03	-4.2									3.14E-10	2.68E-17	2.87E-19								
21H-2	I	Hemipelagic/Pyroclastic	Clay	182.302	0.07	0.09	0.61	0.62	0.26	0.30	0.34	1	0.59	2.25E-03	-4.2	2.46E-10	2.10E-17	2.06E-19								
								0.62	0.29	0.26	0.34	2	0.59	-1.28E-03	2.7	2.21E-10	1.89E-17	5.50E-19								
								0.62	0.27	0.28	0.34	3	0.59	7.79E-04	-1.5	2.45E-10	2.09E-17	1.60E-19								
								0.83	0.30	0.25	0.55	1	0.59	-2.48E-03	5.4	2.11E-10	1.80E-17	2.10E-19								
								0.83	0.26	0.29	0.55	2	0.59	1.40E-03	-2.8	2.27E-10	1.94E-17	4.59E-19								
								0.83	0.28	0.27	0.55	3	0.59	-9.59E-04	1.3	3.44E-10	2.94E-17	5.14E-18								
								0.41	0.26	0.29	0.14	1	0.49	3.54E-04	-2.8	4.00E-11	3.42E-18	6.07E-20								
								0.41	0.30	0.26	0.14	2	0.49	-4.32E-04	4.0	3.44E-11	2.93E-18	6.63E-20								
								0.41	0.25	0.30	0.14	3	0.49	6.42E-04	-5.6	3.69E-11	3.15E-18	2.89E-20								
								38X-2	I	Hemipelagic/Pyroclastic	Clay	284.9	0.06	0.05	0.55	0.41	0.26	0.29	0.14	1	0.54	-1.94E-04	4.0	1.85E-11	1.58E-18	3.95E-20
																0.41	0.26	0.29	0.14	2	0.54	1.03E-04	-2.8	1.39E-11	1.19E-18	4.70E-20
																0.41	0.30	0.25	0.14	3	0.54	-2.30E-04	5.4	1.63E-11	1.39E-18	2.37E-20
0.55	0.29	0.26	0.28	1	0.53	-1.02E-04	2.7									1.49E-11	1.27E-18	1.22E-19								
0.55	0.26	0.30	0.28	2	0.53	1.24E-04	-4.2									1.12E-11	9.60E-19	1.88E-20								
0.55	0.27	0.28	0.28	3	0.53	2.84E-05	-1.5									7.31E-12	6.24E-19	5.40E-20								
0.69	0.30	0.26	0.41	1	0.52	-2.20E-04	4.0									2.13E-11	1.82E-18	1.02E-18								
0.69	0.25	0.30	0.41	2	0.52	2.04E-04	-5.6									1.39E-11	1.19E-18	2.10E-20								
333-C0012E-1X-1	V	Volcaniclastic-rich	Silty clay	500.105	0.06	0.05	0.40									0.41	0.30	0.26	0.14	1	0.39	-1.86E-04	4.0	1.57E-11	1.34E-18	4.84E-20
																0.41	0.26	0.29	0.14	2	0.39	1.14E-04	-2.8	1.36E-11	1.16E-18	1.72E-20
																0.41	0.28	0.27	0.14	3	0.39	-4.99E-05	1.3	1.33E-11	1.13E-18	9.41E-20



Table T1 (continued).

Core, section	Unit/Subunit	Facies	Lithology	Top depth (mbsf)	Diameter (m)	Length (m)	Initial porosity	Confining pressure (MPa)	Top pressure (MPa)	Bottom pressure (MPa)	Effective stress (MPa)	Test	Computed porosity	Flow rate (mL/min)	$\Delta h$ (m)	Hydraulic conductivity (m/s)	Permeability (m <sup>2</sup> )	Standard deviation of $k$ (m <sup>2</sup> )
3X-4	VI	Pelagic clay	Clay	521.845	0.06	0.08	0.37	0.62	0.25	0.30	0.34	1	0.37	1.15E-04	-5.6	7.00E-12	5.98E-19	2.44E-20
								0.62	0.30	0.26	0.34	2	0.37	-1.09E-04	4.0	9.20E-12	7.86E-19	2.97E-20
								0.62	0.28	0.27	0.34	3	0.37	-4.19E-05	1.3	1.11E-11	9.48E-19	9.34E-20
								0.83	0.26	0.29	0.55	1	0.36	5.07E-05	-2.8	6.07E-12	5.18E-19	2.72E-20
								0.83	0.30	0.26	0.55	2	0.35	-1.17E-04	4.0	9.87E-12	8.42E-19	4.96E-20
								0.83	0.25	0.30	0.55	3	0.35	6.71E-05	-5.6	4.08E-12	3.48E-19	1.15E-20
								0.41	0.26	0.29	0.14	1	0.37	3.37E-05	-2.8	5.85E-12	5.00E-19	2.48E-20
								0.41	0.30	0.26	0.14	2	0.37	-8.03E-05	4.0	9.89E-12	8.45E-19	5.66E-20
								0.41	0.27	0.28	0.14	3	0.37	9.36E-06	-1.5	3.14E-12	2.68E-19	5.88E-20
								0.62	0.26	0.30	0.34	1	0.36	1.39E-05	-4.2	1.63E-12	1.39E-19	3.30E-20
								0.62	0.30	0.25	0.34	2	0.36	-4.72E-05	5.4	4.33E-12	3.70E-19	2.63E-20
								0.62	0.24	0.31	0.34	3	0.36	2.95E-05	-7.0	2.10E-12	1.79E-19	7.23E-21
								0.83	0.30	0.25	0.55	1	0.35	-1.08E-04	5.4	9.95E-12	8.50E-19	1.99E-19
								0.83	0.31	0.24	0.55	2	0.35	-7.30E-05	6.8	5.34E-12	4.56E-19	3.54E-20
								0.83	0.29	0.26	0.55	3	0.35	-4.12E-05	2.7	7.72E-12	6.59E-19	7.38E-20
333-C0018A-10H-9	1a	Slope basin	Silty clay	89.012	0.06	0.10	0.57	0.41	0.27	0.28	0.14	1	0.55	3.95E-03	-1.5	1.37E-09	1.17E-16	7.43E-19
								0.41	0.29	0.27	0.14	2	0.55	-5.28E-03	2.0	1.36E-09	1.16E-16	6.70E-19
								0.41	0.26	0.29	0.14	3	0.55	7.37E-03	-2.8	1.31E-09	1.12E-16	5.93E-19
								0.55	0.27	0.28	0.34	1	0.52	2.45E-03	-1.5	8.46E-10	7.22E-17	7.20E-19
								0.55	0.29	0.27	0.34	2	0.52	-2.22E-03	2.0	8.82E-10	7.54E-17	8.50E-19
								0.55	0.26	0.29	0.34	3	0.52	4.22E-03	-2.8	7.51E-10	6.41E-17	1.46E-18
								0.69	0.28	0.27	0.48	1	0.51	-1.95E-03	1.3	7.71E-10	6.58E-17	6.00E-19
								0.69	0.26	0.29	0.48	2	0.51	3.70E-03	-2.8	6.58E-10	5.62E-17	3.05E-19
								0.69	0.30	0.26	0.48	3	0.51	-5.43E-03	4.0	6.79E-10	5.80E-17	1.41E-18

Core types: H = hydraulic piston coring system, X = extended shoe coring system, R = rotary core barrel. More information on the sample code and coring methods can be found in Expedition 333 Scientists (2012a). Lithologic unit designations are from Expedition 322 and 333 (see the “Site C0011” and “Site C0012” chapters [Expedition 322 Scientists, 2010a, 2010b]; Expedition 333 Scientists, 2012b, 2012c, 2012d). Because lithology varies within a facies, a qualitative description of each sample’s grain size is also provided. Italics = results with standard deviation of permeability that exceeds 10% of the computed permeability. A positive flow rate indicates flow from the top to the bottom of the sample, and a negative flow rate indicates flow from the bottom to the top of the sample.